



This is the accepted manuscript made available via CHORUS. The article has been published as:

## High-precision measurements of $\pi p$ elastic differential cross sections in the second resonance region

I. G. Alekseev, V. A. Andreev, I. G. Bordyuzhin, W. J. Briscoe, Ye. A. Filimonov, V. V. Golubev, A. B. Gridnev, D. V. Kalinkin, L. I. Koroleva, N. G. Kozlenko, V. S. Kozlov, A. G. Krivshich, B. V. Morozov, V. M. Nesterov, D. V. Novinsky, V. V. Ryltsov, M. Sadler, B. M. Shurygin, I. I. Strakovsky, A. D. Sulimov, V. V. Sumachev, D. N. Svirida, V. I. Tarakanov, V. Yu. Trautman, and R. L. Workman (EPECUR Collaboration and GW INS Data Analysis Center)

Phys. Rev. C **91**, 025205 — Published 24 February 2015

DOI: [10.1103/PhysRevC.91.025205](https://doi.org/10.1103/PhysRevC.91.025205)

# High-precision measurements of $\pi p$ elastic differential cross sections in the second resonance region

I. G. Alekseev<sup>1</sup>, V. A. Andreev<sup>3</sup>, I. G. Bordyuzhin<sup>1,5</sup>, W. J. Briscoe<sup>2</sup>, Ye. A. Filimonov<sup>3</sup>, V. V. Golubev<sup>3</sup>,  
A. B. Gridnev<sup>3</sup>, D. V. Kalinkin<sup>1</sup>, L. I. Koroleva<sup>1</sup>, N. G. Kozlenko<sup>3</sup>, V. S. Kozlov<sup>3</sup>, A. G. Krivshich<sup>3</sup>,  
B. V. Morozov<sup>1</sup>, V. M. Nesterov<sup>1</sup>, D. V. Novinsky<sup>3</sup>, V. V. Ryltsov<sup>1</sup>, M. Sadler<sup>4</sup>, B.M. Shurygin<sup>1</sup>, I. I. Strakovsky<sup>2</sup>,  
A. D. Sulimov<sup>1</sup>, V. V. Sumachev<sup>3</sup>, D. N. Svirida<sup>1</sup>, V. I. Tarakanov<sup>3</sup>, V. Yu. Trautman<sup>3</sup>, R. L. Workman<sup>2</sup>

(EPECUR Collaboration and GW INS Data Analysis Center)

<sup>1</sup>*Institute for Theoretical and Experimental Physics, Moscow, 117218, Russia*

<sup>2</sup>*The George Washington University, Washington, DC 20052, USA*

<sup>3</sup>*Petersburg Nuclear Physics Institute, Gatchina, 188300, Russia*

<sup>4</sup>*Abilene Christian University, Abilene, Texas, TX 79699-7963, USA and*

<sup>5</sup>*National University of Science and Technology "MISiS", Moscow, 119049, Russia*

(Dated: January 15, 2015)

Cross sections for  $\pi^\pm p$  elastic scattering have been measured to high precision by the EPECUR Collaboration for beam momenta between 800 and 1240 MeV/c using the ITEP proton synchrotron. The data precision allows comparisons of the existing partial-wave analyses on a level not possible previously. These comparisons imply that, over the covered energy range, the Carnegie-Mellon-Berkeley analysis is significantly more predictive when compared to versions of the Karlsruhe-Helsinki analyses.

PACS numbers: 12.40.Vv,13.60.Le,14.40.Be,25.20.Lj

Measurements of  $\pi p$  elastic differential cross sections by the EPECUR group, at the ITEP 10 GeV proton synchrotron, have produced data of unprecedented precision for beam momenta from 800 to 1243 MeV/c (producing 4277  $\pi^- p$  data) and from 918 to 1240 MeV/c (producing 2638  $\pi^+ p$  data). In measuring the  $\pi^\pm p \rightarrow \pi^\pm p$  differential cross sections, all event candidates were divided into 66 ( $\pi^+ p$ ) and 107 ( $\pi^- p$ ) incident momentum bins. The data within each momentum bin were divided into 40 pion central-of-mass scattering angle (c.m.) ( $\theta$ ) bins, from 40 to 122 degrees. This momentum range covered center-of-mass energies from 1560 to 1800 MeV, spanning a significant portion of the resonance region.

The precision greatly exceeds that of previously available cross sections, which were used to generate the Karlsruhe-Helsinki [1, 2] (KH) and Carnegie-Mellon-Berkeley [3] (CMB) fits, from which much of non-strange baryon spectrum was determined. This addition thus allows a comparison of the classical KH and CMB analyses, and the more recent GW results [4], at a level that was not possible with the previously existing database.

Below, we first describe the experimental design and analysis. We then outline cases where a clear distinction exists between the new data and some of these older analyses.

The layout of the experiment [5] is shown in Fig. 1. This is a two-arm non-magnetic spectrometer placed in the second focus of a universal high-resolution secondary beam line of the ITEP proton synchrotron. The first focus of the beam line is equipped with a set of four 2-coordinate proportional chambers (**1FCH1-4** in Fig. 1) with 1 mm pitch, which allows the tagging of each beam particle with its momentum with a precision of about 0.1%. A similar set of proportional chambers (**2FCH1-4**) is placed in the second focus in front of the target.

Beam size ( $\sigma$ ) at the target is 5.5 mm and 3.5 mm in the horizontal and vertical planes respectively. A “magic” (argon-isobutane-freon) gas mixture is used in proportional chambers. Beam tests showed better than 99% efficiency. The liquid hydrogen reservoir of the target is made of mylar and has a 40 mm diameter and a length of about 250 mm along the beam. The reservoir is placed in a vacuum-tight 80 mm diameter beryllium outer shell with a mylar covered window on the beam entrance flange. Scattered particles are measured by two symmetrical arms of drift chambers (**DC1-8**) with hexagonal structure. Each arm consists of 4 chambers. Wires in odd-numbered chambers are horizontal, with even-numbered wires being vertical. Each chamber has 2 sensitive wire planes with a 17 mm pitch. The planes are shifted by half of the pitch. The two chambers closest to the target have a sensitive area of  $600 \times 400 \text{ mm}^2$ . Six other chambers have a sensitive area of  $1200 \times 800 \text{ mm}^2$ . A gas mixture of 70% Ar and 30% CO<sub>2</sub> is used in the drift chambers. Beam tests showed better than 99% single drift plane efficiency with 0.2 mm resolution for perpendicular tracks.

The central beam momentum was calibrated with 0.1% precision at three values: 1057, 1095, and 1297 MeV/c using protons of the internal accelerator beam elastically scattered on the beryllium target. The field of the last dipole magnet of the beam line is controlled by NMR, providing stability of the energy calibration. In addition to the pions, the beam contains also electrons (positrons), muons and protons (for the positive beam). Contamination from other particles (kaons and anti-protons) is negligible. Protons were rejected at the trigger level by time-of-flight between scintillator counters in the first and the second focuses. The residual proton contamination was checked using the difference

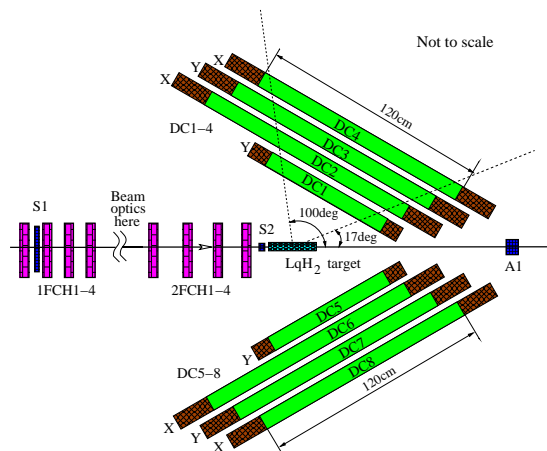


FIG. 1. (Color on-line) The experimental setup (top view). **1FCH1-4** and **2FCH1-4** — 1-mm pitch proportional chambers, **DC1-DC8** — drift chambers, **LH<sub>2</sub>** — liquid hydrogen target, **S1**, **S2** and **A1** — trigger scintillation counters.

between  $pp$  and  $\pi p$  elastic kinematics and was found to be less than 0.2%. The contribution of electrons and muons was measured using a gas Cherenkov counter and simulated using Geant4 [6]. The fraction of electrons (positrons) is about 3% at 840 MeV/c, falling approximately linearly to 1.5% at 1240 MeV/c. The fraction of muons falls, over this range, from 6% to 4%.

A unique distributed DAQ system, based on the commercial 480 Mbit/s USB 2.0 interface, was designed for the experiment [7]. It consists of 100-channel boards for proportional chambers and 24-channel boards for drift chambers, placed on the chamber frames. Trigger logic is capable of processing several trigger conditions activating different sets of detectors. DAQ features nearly dead-time-less operation and can process up to  $10^5$  events per spill. A soft trigger condition was used to acquire physics events:

$$T = S_1 \cdot S_2 \cdot M_{1FCH} \cdot M_{2FCH} \cdot \overline{A_1}, \quad (1)$$

where  $S_1$ ,  $S_2$ , and  $A_1$  are signals from corresponding scintillation counters and  $M_{1FCH}$  and  $M_{2FCH}$  are fast signals from the proportional chamber blocks in the 1<sup>st</sup> and the 2<sup>nd</sup> focuses. Other trigger conditions with large prescale were used for beam position and luminosity monitoring. During data taking the momentum range was scanned with 15 MeV/c steps in the central momentum of the beam, which is about one half of the momentum spread in each step.

Selection of the elastic events in this experiment is based on the angular correlation of pion and proton tracks. A single track is required in the beam chambers and both scattering arms. All of these tracks are required to form a common vertex inside the target (5 mm from mylar walls at least) and lie in a plane. A central-of-mass scattering angle,  $\theta$ , is calculated for both scattered particles under the assumption that the pion has scattered to the left. A distribution of the events over the dif-

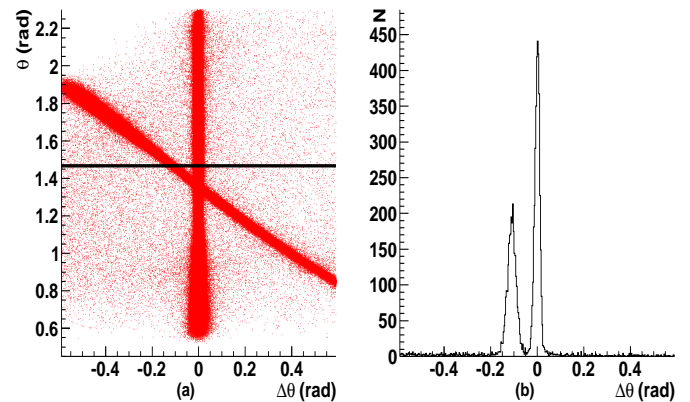


FIG. 2. (Color on-line) 2-dimensional distribution over the difference between calculated center of mass scattering angles for pion and proton, assuming that the pion goes to the left arm,  $\Delta\theta$  (absciss) and the scattering angle  $\theta$  (ordinate) - (a) and its slice at  $\theta = 84$  degree (b).

ference between reconstructed scattering angles  $\Delta\theta$  and the scattering angle  $\theta$  is shown in Fig. 2a for one beam momentum setting. Two clusters are clearly seen. One corresponds to the pion scattered to the left (the assumption was correct) and the other corresponds to the pion scattered to the right (the assumption was wrong). A slice of the distribution for a one degree  $\theta$  interval  $\theta = 84$  degree is shown in Fig. 2b. This figure also illustrates the amount of inelastic background, which was calculated and subtracted in each bin. Differential cross sections were calculated from the number of elastic events corrected for acceptance and chamber efficiency. Beam monitoring is based on a special trigger, which ignores counter  $A_1$ , used as a veto in the main trigger. This trigger has exactly the same dead time as the main trigger, so no correction for the dead time in the analyses is necessary. Numeric characteristics of the data sample are presented in Table I.

TABLE I. Parameters of the statistics presented

|                                | $\pi^- p \rightarrow \pi^- p$ | $\pi^+ p \rightarrow \pi^+ p$ |
|--------------------------------|-------------------------------|-------------------------------|
| $\theta$ angle range (degrees) | 40 – 122                      | 40 – 122                      |
| Beam momentum range (GeV/c)    | 0.80 – 1.24                   | 0.92 – 1.24                   |
| Triggers accumulated           | $1.25 \cdot 10^9$             | $0.69 \cdot 10^9$             |
| Elastic events                 | $2.24 \cdot 10^7$             | $1.48 \cdot 10^7$             |

The main systematic error contributions are listed in Table II. We estimate the total systematic uncertainty to be 2.6%, combining the sum of tabulated uncertainties in quadrature.

Cross section data with a fine energy grid and high precision have been achieved. These cross sections have placed far higher constraints on existing partial-wave analysis (PWA) than any previous experiment. As a result, angular structures are extremely well defined and clearly differentiate between the classic analyses of the KH [1, 2], CMB [3], and GW DAC [4] groups.

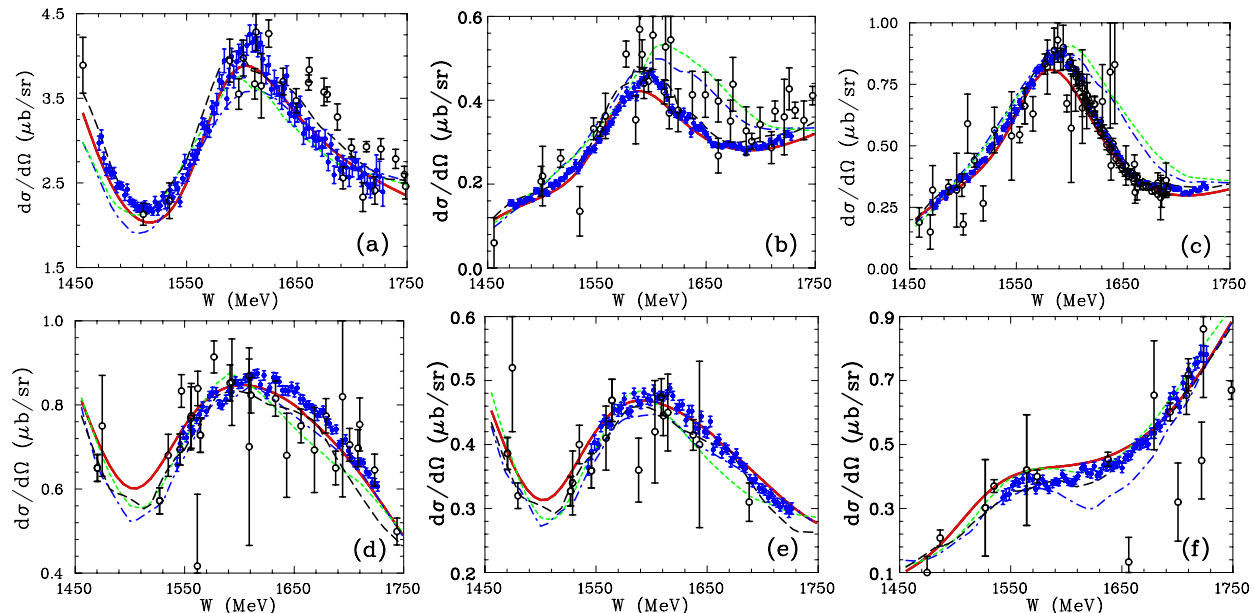


FIG. 3. (Color on-line) Differential cross sections for selected angles in the center-of-mass frame,  $\theta$ , for  $\pi^-p \rightarrow \pi^-p$  [top panel: (a)  $\theta = 40$  degree, (b)  $\theta = 100$  degree, and (c)  $\theta = 110$  degree] and  $\pi^+p \rightarrow \pi^+p$  [bottom panel: (d)  $\theta = 70$  degree, (e)  $\theta = 80$  degree, and (f)  $\theta = 120$  degree]. New EPECUR data (statistical errors only) are plotted as blue filled circles with previous measurements presented as black open circles. The data from earlier experiments (statistical errors only) are within bins of  $\Delta\theta = \pm 1$  degree [8]. An existing GW INS DAC fit, WI08 [4], is plotted with a red double solid curves while the older KH80 [1], KA84 [2], and CMB [3] fits are plotted as blue dash-dotted, green short dashed, and black dashed curves, respectively. New EPECUR data do not include in any presented fits.

TABLE II. Systematic errors

| Systematic error origin                   | Base for the estimation  | Error |
|---|--|-------|
| Beam pollution with electrons and muons   | Comparison of Monte-Carlo and Cherenkov counter measurements   | 1%    |
| Luminosity normalization                  | Comparison of elastic events yield for all angles in the overlapping momentum ranges   | 2%    |
| Tracking efficiency and setup geometry    | Comparison of cross sections obtained for events with a pion hitting the left arm to those with a pion hitting the right arm | 1%    |
| Monte-Carlo simulations of the acceptance | Comparison of two independently applied acceptance simulations   | 0.8%  |
| Various cuts used in the analysis         | Dependence of the event yield on the cut   | 0.5%  |

In Fig. 3, we plot several fixed-angle cross sections for elastic  $\pi^-p$  and  $\pi^+p$  scattering, and compare with both the older datasets and the predictions based on fits to these older data. Using only the older less-precise and often contradictory data, as displayed in the figures, none of the existing fits can claim to give a superior description. However, the present set of higher-precision data can, in some cases, clearly select the older CMB [3] and recent GW DAC fits [4] over the KH80 [1] and KA84 [2] fits.

In Fig. 4, we compare the data predictions in terms of  $\chi^2/\text{data}$  for the KH, CMB, and GW DAC fits. Here also it is clear that the CMB prediction is amazingly good, considering that the fit was based on the less-precise data shown in the figures. In order to better accommodate for systematic uncertainty in experiments at each energy, a normalization factor was allowed for the corresponding angular distribution. The normalization factor,  $N$ , contributed an addition term to  $\chi^2$ ,  $[(N-1)/\epsilon]^2$ , with  $\epsilon$  being the overall systematic error. This contribution was

typically less than 10% of the total value plotted in the figure.

While there are many overlapping resonances contributing to the plotted  $\pi^-p$  data, for  $\pi^+p$  (isolating the isospin 3/2 contribution) there are only a couple of 4-star states. These are plotted along with their elastic and total widths in the Fig. 4. While it may be tempting to associate the  $\chi^2$  peak for KH, near the energy of the  $\Delta(1620)$  with a resonance description different from the CMB fit, this can be effectively ruled out, because resonance parameters from the analyses are very close. The  $\Delta(1620)$  pole parameters (Real part,  $-2 \times$  Imaginary part) are (1608, 116) MeV for KH and  $(1600 \pm 15, 120 \pm 20)$  MeV for CMB, whereas the pole residues (modulus, phase) are, respectively, (19 MeV,  $-95$  degree) and  $(15 \pm 2 \text{ MeV}, -110 \pm 20 \text{ degree})$ .

Figure 4 also displays a fit to the new data using the parameterization of the original WI08 fit. This exercise produced a fit by mainly adjusting the renormalization

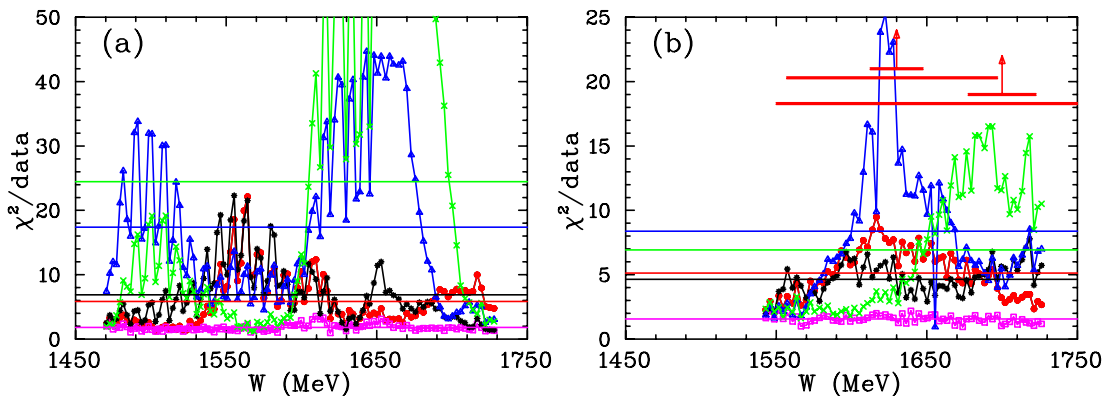


FIG. 4. (Color on-line) Comparison of  $\chi^2/\text{data}$  distributions covered  $W = 1450 - 1750$  MeV, (a)  $\pi^- p \rightarrow \pi^- p$  and (b)  $\pi^+ p \rightarrow \pi^+ p$ . An existing GW INS DAC fit, WI08 [4], is plotted with a red double filled circles while the older KH80 [1], KA84 [2], and CMB [3] fits are plotted as blue filled triangles, green crosses, and black stars, respectively. The new SAID WI14 solution (including new EPECUR data) shown by magenta open squares. Horizontal lines show average value of  $\chi^2/\text{data}$  for associated solution. The curves are added to guide the eye. On the right plot, vertical arrows indicate resonance energies  $W_R$  and horizontal bars show full ( $\Gamma$ ) and partial ( $\Gamma_{\pi N}$ ) widths ( $I = 3/2$ ) associated with the SAID  $\pi N$  solution WI08 [4].

factors mentioned above in calculating  $\chi^2$ . The resulting changes in the amplitudes were very slight. A detailed discussion of the GW DAC fit procedure is provided in Refs. [4, 9].

In a previous SAID analysis, a scan for narrow resonances was made over the present energy range [13]. For an energy of about 1680 MeV, this possibility was not excluded, based on existing data. Indeed, several independent experiments on eta-neutron photoproduction have found a narrow peak at this mass (a recent brief review of its status is given in Ref. [10]). Our present measurements and their preliminary analysis (WI14) do not reveal a clear manifestation of any such resonance. Though some indications of narrow structures may be

seen [11, 12], their nature require further investigation. It has been emphasized [13] that the coupling of a purported  $N(1680)$  state to the  $\pi N$  channel should be suppressed. A more extensive analysis would involve multi-channel fits with analytically built-in thresholds for opening channels. Work in this direction is planned, based on the Jülich and Gatchina models of pion-induced reactions [12, 14].

The authors wish to acknowledge the excellent support of the accelerator group and operators of ITEP. This work was partially supported by Russian Fund for Basic Research grants 09-02-00998a and 05-02-17005a and by the U.S. Department of Energy, Office of Science, Office of Nuclear Physics, under Award Number DE-FG02.99ER41110.

- 
- [1] G. Höhler, *Pion Nucleon Scattering*, Part 2, Landolt-Bornstein, Vol.9b, 1983.
- [2] R. Koch, *Z. Phys. C* **29**, 597 (1985).
- [3] R. E. Cutkosky *et al.*, *Phys. Rev. D* **20**, 2839 (1979); R. E. Cutkosky in *Proceedings of the 4th Conference on Baryon Resonances*, ed. N. Isgur, (Toronto, 1983).
- [4] R. L. Workman, R. A. Arndt, W. J. Briscoe, M. W. Paris, I. I. Strakovsky, *Phys. Rev. C* **86**, 035202 (2012); R. A. Arndt, W. J. Briscoe, I. I. Strakovsky, and R. L. Workman, *Phys. Rev. C* **74**, 045205 (2006).
- [5] I. G. Alekseev *et al.*, *Instrum. Exp. Tech.* **57**, 535 (2014); I. G. Alekseev *et al.*, arXiv:0509032 [hep-ex].
- [6] S. Agostinelli *et al.* (Geant4 Collaboration), *Nucl. Instrum. Meth. A* **506** 250 (2003); <http://geant4.cern.ch/>
- [7] I. G. Alekseev *et al.*, *Nucl. Instrum. Meth. A* **578** 289 (2007).
- [8] W. J. Briscoe, D. Schott, I. I. Strakovsky, and R. L. Workman, Institute of Nuclear Studies of the George Washington University Database; <http://gwdac.phys.gwu.edu/>.
- [9] R. A. Arndt, I. I. Strakovsky, R. L. Workman, and M. M. Pavan, *Phys. Rev. C* **52**, 2120 (1995).
- [10] Ya I. Azimov and I. I. Strakovsky, *Proceedings of the XVth International Conference on Hadron Spectroscopy (Hadron 2013)*, Nara, Japan, Nov. 2013, *Proceedings of Science (Hadron 2014)* 034.
- [11] I. G. Alekseev *et al.*, *Int. J. Mod. Phys. Conf. Ser.* **26**, 1460076 (2014).
- [12] A. B. Gridnev, *Proceedings of the XVth International Conference on Hadron Spectroscopy (Hadron 2013)*, Nara, Japan, Nov. 2013, *Proceedings of Science (Hadron 2014)* 099.
- [13] R. A. Arndt *et al.*, *Phys. Rev. C* **69**, 035208 (2004).
- [14] M. Döring and K. Nakayama, *Phys. Lett. B* **683**, 145 (2010).